Open Access on 05/13/2015

ARTICLE

Ultra-High Throughput Synthesis of Nanoparticles with Homogeneous Size Distribution Using a Coaxial Turbulent Jet Mixer

Jong-Min Lim,[†,‡,§] Archana Swami,[‡] Laura M. Gilson,[†] Sunandini Chopra,[†] Sungyoung Choi,[†,⊥] Jun Wu,[‡] Robert Langer,[§,∥] Rohit Karnik,[†,*] and Omid C. Farokhzad[‡,#,*]

[†]Department of Mechanical Engineering, Massachusetts Institute of Technology, Cambridge, Massachusetts 02139, United States, [‡]Laboratory of Nanomedicine and Biomaterials, Department of Anesthesiology, Brigham and Women's Hospital, Harvard Medical School, Boston, Massachusetts 02115, United States, [§]David H. Koch Institute for Integrative Cancer Research, Massachusetts Institute of Technology, Cambridge, Massachusetts 02139, United States, [⊥]Department of Biomedical Engineering, Kyung Hee University, 1732 Deogyeong-daero, Giheung-gu, Yongin-si, Gyeonggi-do 446-701, Republic of Korea, [∥]Department of Chemical Engineering, Massachusetts Institute of Technology, Cambridge, Massachusetts 02139, United States, and [#]King Abdulaziz University, Jeddah 22254, Saudi Arabia

ABSTRACT High-throughput production of nanoparticles (NPs) with controlled quality is critical for their clinical translation into effective nanomedicines for diagnostics and therapeutics. Here we report a simple and versatile coaxial turbulent jet mixer that can synthesize a variety of NPs at high throughput up to 3 kg/d, while maintaining the advantages of homogeneity, reproducibility, and tunability that are normally accessible only in specialized microscale mixing devices. The device fabrication does not require specialized machining and is easy to operate. As one example, we show reproducible, high-throughput formulation of siRNA-polyelectrolyte polyplex NPs that exhibit effective gene knockdown but exhibit significant dependence on batch size when formulated using conventional methods. The coaxial turbulent jet mixer can accelerate the development of nanomedicines by providing a robust and versatile platform for preparation of NPs at throughputs suitable for *in vivo* studies, clinical trials, and industrial-scale production.

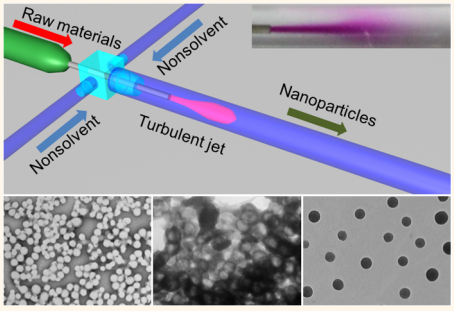

KEYWORDS: nanoparticles · mixer · turbulent jet · nanomedicine · nanoprecipitation · rapid mixing · large-scale · microfluidics

Nanoparticles (NPs) have shown great promise in the rapidly evolving field of nanomedicine as nanocarriers for drug delivery,[1,2] for fluorescence imaging,[3,4] and as contrast agents for magnetic resonance imaging (MRI).[5] Indeed, NPs approved by the Food and Drug Administration (FDA) are currently in use for treatment of metastatic adenocarcinoma of pancreas (Abraxane, a protein-based carrier), ovarian cancer that has progressed or recurred after platinum-based chemotherapy (Doxil, a liposome-based carrier), and for MRI of liver (Ferumoxide, dextran-coated iron oxide NPs).[2,6] In addition, a polymeric micelle NP (Genexol-PM) was approved in Korea and is in phase II clinical development in the USA,[2,6] while the first targeted poly(lactide-*co*-glycolide)-*b*-poly(ethylene glycol) (PLGA–PEG) NPs have successfully completed phase I clinical trials and advanced to phase II clinical trials for prostate cancer therapy.[7]

Despite these advances, translation of NPs from the bench to bedside is difficult; among the major challenges is controlling the properties and quality of NPs from laboratory scale synthesis to the clinical production scale.[1] While NPs are conventionally synthesized by batch type reactors, these bulk synthesis methods tend to have limited batch-to-batch reproducibility and controllability in terms of physicochemical properties of the synthesized NPs.[8] In addition, the scaling up of batch procedures for industrial-scale production needs considerable trial and error for process optimization.[9] Because the *in vivo* fate of NPs strongly depends on their physicochemical properties,[1,2,7] methods to synthesize NPs in a reproducible and controlled manner from

* Address correspondence to karnik@mit.edu, ofarokhzad@zeus.bwh.harvard.edu.

Received for review March 10, 2014 and accepted May 13, 2014.

Published online May 13, 2014
10.1021/nn501371n

laboratory-scale *in vitro* screening studies all the way to production scale are critical for the development and translation of NPs to the clinic.

Continuous synthesis of NPs typically provides better reproducibility and controllability compared to batch-type bulk synthesis methods.[10−12] Recently, the ability of microfluidic platforms to offer precisely controlled reaction environments has been harnessed to enhance the controllability and reproducibility of NP synthesis.[1,2,9,11,13] Controlled synthesis of NPs through nanoprecipitation by rapid mixing in microfluidic platforms has been shown to improve the homogeneity of polymeric NPs.[11,14−21] Microfluidic platforms have also been used for tuning the physicochemical properties of NPs including size, surface chemistry, surface charge, and targeting agent density,[16,18,21,22] and have enabled rapid screening of the synthesized NPs.[22]

However, the requirement for specialized microfabrication facilities, lack of robustness, and know-how required to operate the devices creates a barrier for their utilization in biomedical research laboratories that often do not have microdevice expertise. Moreover, only a handful of organic solvents are compatible with conventional polydimethylsiloxane (PDMS) microfluidic systems.[23] Their productivity is also typically low (<0.3 g/h),[20,21] which considerably falls short of the production rates typically required in clinical studies and industry. While millifluidic systems including confined impinging jet mixer[14,24] and multi-inlet vortex mixer[25] have been used for the synthesis of NPs, specialized micromachining[14,24,25] is still required. As a consequence, the full potential of these devices for controlled and tunable synthesis of homogeneous NPs remains unrealized.

Here we demonstrate a simple and versatile coaxial turbulent jet mixer for synthesizing NPs with high production rates up to 3 kg/d suitable for *in vivo* studies, clinical trials, and industrial-scale production, while retaining the advantages of homogeneity, reproducibility, and control over NP properties. More importantly, the coaxial turbulent jet mixer can be prepared in half an hour with off-the-shelf components and a drill. We demonstrate the versatility of the coaxial turbulent jet mixer by preparing various types of NPs including PLGA−PEG NPs,[16,19,21] lipid vesicles,[15,17] iron oxide NPs,[26] polystyrene NPs,[24] and siRNA-polyelectrolyte (Polyethylenimine: $PEI_{25k,Branched}$) polyplex NPs[27] by rapid nanoprecipitation and encapsulating different functional agents including anticancer drug, insulin, fluorescent dyes, and siRNA.

RESULTS

The coaxial turbulent jet mixer consists of coaxial cylindrical tubes where NP precursors and nonsolvent are injected through the inner and outer tubes, respectively (Scheme 1). The coaxial turbulent jet mixer is prepared by inserting a blunt syringe needle into a "T"

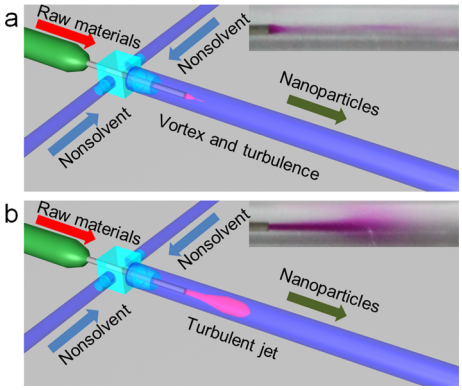

Scheme 1. Schematic illustration of the coaxial turbulent jet mixer for high-throughput synthesis of NPs. Schematic illustration of the coaxial turbulent jet mixer with (a) turbulence induced by vortex and (b) turbulence induced by jetting. The insets show the top view of the turbulent jets (a) when R = 0.3 and Re = 353, and (b) when R = 10 and Re = 1311, respectively.

tube fitting. Fabrication can be accomplished within 30 min without requiring specialized equipment, microfabrication facilities, or specialized skills. In addition, the coaxial turbulent jet mixer is reusable and the needle is easily replaceable as needed. While a wide choice of standard fittings and materials can be used to construct the coaxial turbulent jet mixer, we used PTFE fittings and tubing that are compatible with a variety of solvents (Figure 1a). When operated at high flow rates, the device rapidly mixes the injected solutions by the formation of a turbulent jet. Because of the rapid solvent exchange, uniform NPs can be synthesized by self-assembly of the precursors through a process known as nanoprecipitation.[14,16,19,21]

Flow Regimes and Mixing Time Scale. Understanding the flow behavior and mixing time (τ_{mix}) in the coaxial turbulent jet mixer is important because NP assembly is strongly influenced by τ_{mix}.[14,16] Fluid flow in the coaxial turbulent jet mixer is defined by two dimensionless parameters:[28] flow velocity ratio $R = u_i/u_o$, and the average Reynolds number $Re = QD/\nu A$, where u_i and u_o are input velocities of inner stream and outer stream, Q and ν are total flow rate and kinematic viscosity of the fluid mixture, and D and A are the diameter and cross-sectional area of outer tube, respectively. The velocity ratio defines how fast the inner fluid emerges relative to the outer fluid, while the Reynolds number captures the effect of fluid inertia relative to viscous forces. In our experiments, flow rates of inner (Q_i) and outer (Q_o) fluid streams were controlled by using syringe pumps to vary Re and R (Supporting Information eq S1 and S2).

Fluid flow and mixing in the device was visualized using a phenolphthalein solution as the inner fluid, which becomes colorless upon mixing with the acidic outer stream (Figure 1b). The flow behavior was categorized into laminar, transition, vortex and turbulence, and turbulent jet regimes as summarized in the

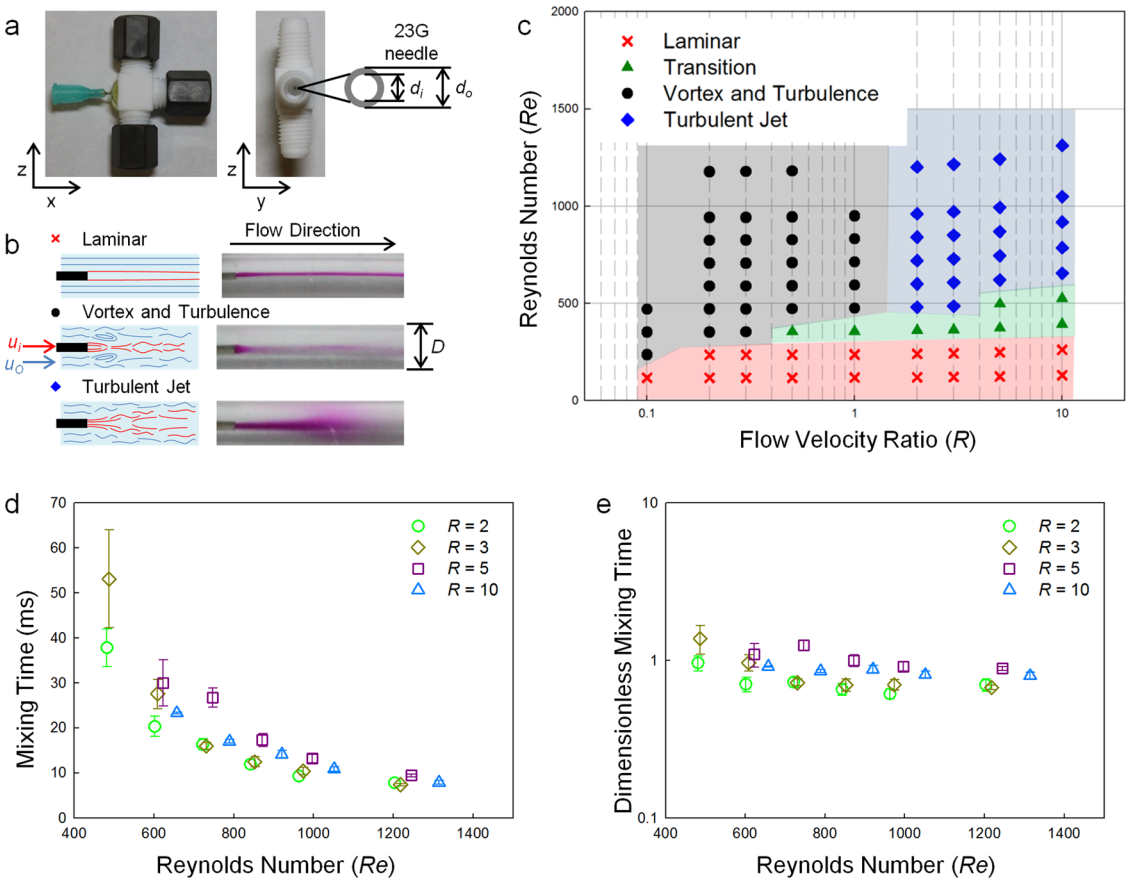

Figure 1. Coaxial turbulent jet mixer and analysis of flow regimes and mixing time (τ_{mix}). (a) Photograph of coaxial turbulent jet mixer fabricated from PTFE tee union tube fittings. (b) Schematic illustrations and top views of fluid flow at laminar ($R = 1$ and $Re = 237$), vortex and turbulence ($R = 0.3$ and $Re = 353$), and turbulent jet ($R = 10$ and $Re = 1311$) regimes. (c) Phase diagram of jet flow regime in terms of R and Re. (d) τ_{mix} and (e) dimensionless mixing time as a function of Re when the coaxial turbulent jet mixer is operated in turbulent jet regime (*i.e.*, $R > 1$ and Re is large). Error bars denote ± s.d.

phase diagram (Figure 1c) obtained by analyzing the flow images (Figure 1b) and videos (Supporting Information Video S1). When $R < 1$, the inner fluid is focused by the outer fluid and the lower velocity of the inner fluid stream at the tip of the needle creates recirculating vortices at low Re. Mixing time is difficult to quantify in this regime due to entrainment of the fluid in vortices. In this regime the flow rate of the inner fluid is very low ($Q_i \lesssim 0.01\ Q_o$), making it less desirable for NP synthesis. This regime transitions to vortices and turbulence at higher Re, where a microvortex is generated at the tip of the needle and turbulence is developed downstream. At higher velocity ratios ($R \gtrsim 1$), the flow remains laminar at low Re and a stable stratified flow is maintained. Because slow diffusional mixing is dominant in the laminar flow regime, the fluid is not completely mixed. As the Re increases, the flow becomes unstable and fluctuates between laminar and turbulent flows in the transition regime, and finally changes to a completely turbulent jet regime that is desirable for NP synthesis due to rapid mixing and favorable flow rate ratios ($Q_i \gtrsim 0.02\ Q_o$).

In the turbulent jet regime, we estimated the mixing time (τ_{mix}) by quantifying the mixing length (L) where the phenolphthalein color transitioned to 90% of its fully mixed value (Supporting Information Figure S1). Assuming that the fluid flows at an average velocity u_{avg} (Supporting Information eq S3), τ_{mix} can be estimated as

$$\tau_{mix} = \frac{L}{u_{avg}} \quad (1)$$

Operating in turbulent jet regime, the τ_{mix} was tunable in the range of 7−53 ms by changing Re, with faster mixing occurring at higher Re (Figure 1d).

To theoretically capture the mixing time scale, we use the engulfment, deformation, diffusion (EDD) turbulent micromixing model.[28] In the EDD model, the unmixed fluid first enters turbulent vortices that stir the fluid at their characteristic frequency, leading to folding of the fluid into a layered structure. The layers become thinner with time, and molecular diffusion finishes the mixing process once the layers are sufficiently thin.[28] The characteristic time scale (τ_ω) in EDD turbulent micromixing model is given by

$$\tau_\omega \approx 12.7\left(\frac{\nu}{\langle\varepsilon\rangle}\right)^{0.5} \quad (2)$$

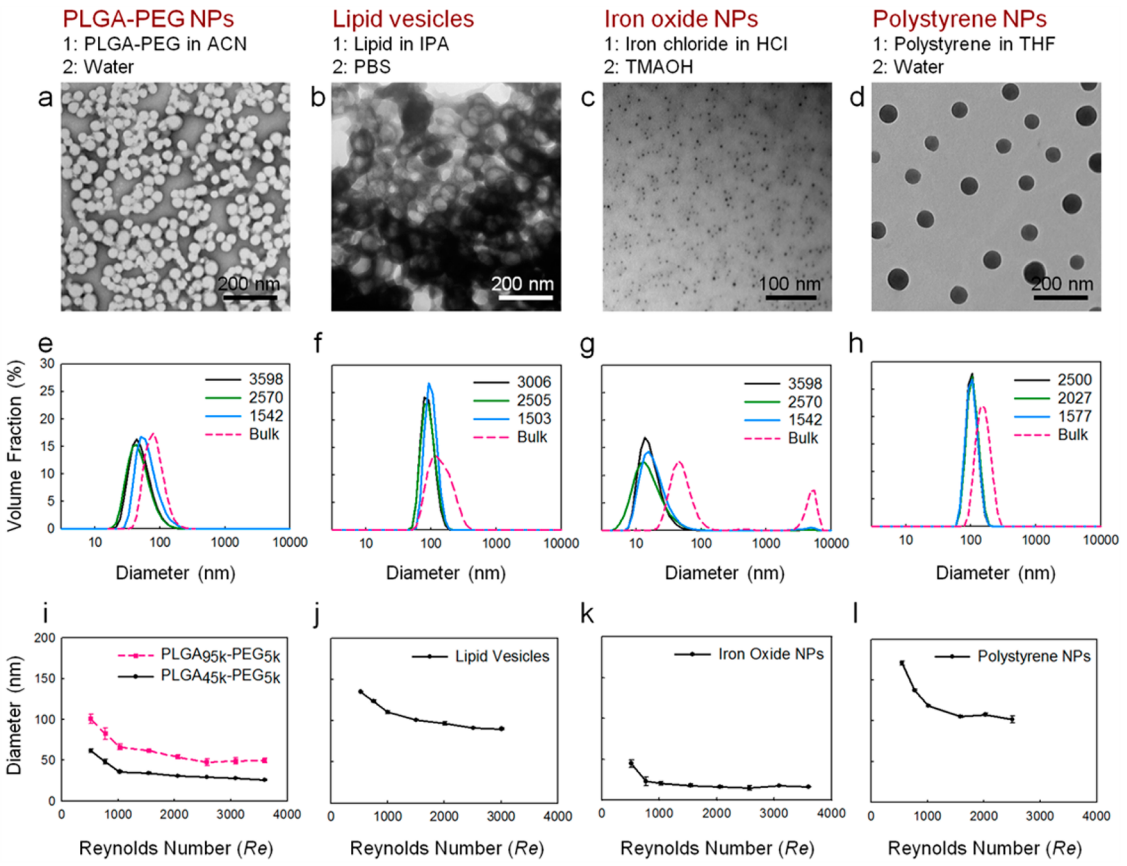

Figure 2. NPs prepared using the coaxial turbulent jet mixer. (a−d) TEM images, (e−h) size distribution by volume fraction, and (i−l) effect of *Re* on the size of (a,e,i) $PLGA_{95k}$-PEG_{5k} NPs, (b,f,j) lipid vesicles, (c,g,k) iron oxide NPs, and (d,h,l) polystyrene NPs, respectively. The NP precursors (1) and nonsolvents (2), introduced as inner and outer fluid streams, respectively, are listed at the top. Error bars denote ± s.d.

where ν is the kinematic viscosity and $\langle\varepsilon\rangle$ is the average turbulent kinetic energy dissipation rate in the core of the pipe flow, given by

$$\langle\varepsilon\rangle = 0.0668\,\frac{u_{avg}^3}{Re^{0.25}D} \qquad (3)$$

Normalizing τ_{mix} by τ_ω collapses the mixing time to a value of unity independent of *R* and *Re* (Figure 1e), demonstrating that the mixing time can be estimated by the EDD model when the coaxial turbulent jet mixer is operated in turbulent jet regime.

Versatile Synthesis of Nanoparticles. The coaxial turbulent jet mixer is a versatile platform that can synthesize a variety of NPs in a reproducible, controlled, and high-throughput manner. As proof of concept, we synthesized various NPs that are commonly used for biomedical applications, including PLGA−PEG NPs, lipid vesicles, iron oxide NPs, polystyrene NPs, and siRNA/PEI polyplex NPs (Figure 2).

The size distributions of NPs prepared using coaxial turbulent jet mixer were narrower and the NPs were smaller than those prepared by conventional bulk synthesis methods, as confirmed by both transmission electron microscope (TEM) images (Figure 2a−d and Supporting Information Figure S2) and dynamic light scattering (Figure 2e−h and Supporting Information Figure S2). The diameter obtained from dynamic light scattering is consistent with that obtained from TEM images in the case of PLGA−PEG NPs. Dynamic light scattering yields a larger diameter for iron oxide NPs due to dipole−dipole interactions,[29] but even in this case TEM analysis reveals a tighter distribution of NP sizes compared to bulk synthesis (Supporting Information Figure S2). The formation of smaller and more homogeneous NPs occurs because mixing in the coaxial turbulent jet mixer is more precisely controlled than that in bulk synthesis and τ_{mix} is smaller than the characteristic aggregation time scale (τ_{agg}). This behavior is consistent with previous reports of nanoprecipitation using microfluidic devices.[14,16,17,19,21] For example, the polystyrene NPs prepared by coaxial turbulent jet mixer were more uniform in size distribution compared to commercially available polystyrene NPs synthesized by emulsion polymerization method (Supporting Information Figure S3).

The size of NPs could be controlled reproducibly by simply changing *Re*. Operating in turbulent jet regime, τ_{mix} is tunable by changing the *Re*, with faster mixing at higher *Re* (Figure 1d). By simply changing *Re*, the size of PLGA−PEG NPs could be controlled reproducibly in

the range of 25−60 nm and 50−100 nm for $PLGA_{45k}$-PEG_{5k} and $PLGA_{95k}$-PEG_{5k}, respectively, with smaller NPs being produced at higher *Re* (Figure 2i). Similar to the case of PLGA−PEG NPs, the size of lipid vesicles, iron oxide NPs, and polystyrene NPs could be controlled precisely and reproducibly by simply changing *Re*, with smaller size occurring at higher *Re* (Figure 2j−l). The influence of τ_{mix} on the size of NPs plateaued beyond a certain *Re*, suggesting that these NPs had reached the size corresponding to the limit of rapid mixing.[14,21]

The coaxial turbulent jet mixer provides an inherently high NP production throughput due to operation in the turbulent regime with device dimensions in the millimeter scale, which involves high *Re* and high flow rates. Typical *Re* in the coaxial turbulent jet mixer ranged from 500 to 3500 (Figure 2i−l and Table 1). Assuming that all the NP precursors flowing into the device are essentially converted to NPs,[20] in case of PLGA−PEG NPs we estimate production rates up to 2.19 g/min (~3.15 kg/d) when the coaxial turbulent jet mixer is operated at high *Re* (*i.e.*, *Re* = 3598) and high polymer concentrations (*i.e.*, 50 mg/mL) (Table 1 and Supporting Information Video S2). Since the coaxial turbulent jet mixer operates in continuous mode, we expect that the quality of NPs will be independent of batch size. To examine the effect of aggregation of precipitates on NP synthesis, we prepared $PLGA_{95k}$-PEG_{5k} NPs where the high molecular weight hydrophobic PLGA block tends to promote aggregation on the channel walls.[19] We observed that the size distribution of $PLGA_{95k}$-PEG_{5k} NPs was essentially identical within standard error for the tens of milligram synthesis scale and for a few gram scale (Supporting Information Figure S4), illustrating the robustness of the coaxial turbulent jet mixer.

Encapsulation of Functional Agents. Polymeric NPs have received considerable attention in the field of nanomedicine as practical platforms for targeted delivery of therapeutic and diagnostic agents.[30,31] NPs loaded with imaging agents also have the potential for improved sensitivity and photostability compared to conventional imaging agents.[3,4] The coaxial turbulent jet mixer easily allows for encapsulation of a variety of functional agents in NPs by simply including them in the precursor solution.

We encapsulated docetaxel and insulin in PLGA−PEG NPs as model therapeutic agents for cancer and diabetes, respectively, by premixing them in the NP precursor solution (Figure 3a−d). In both cases, we did not observe significant changes in the size distribution of PLGA−PEG NPs when the model therapeutic agents were encapsulated (Figure 3a,c). Drug loading, defined as the mass fraction of drug in the NPs, and encapsulation efficiency, the fraction of initial drug that is encapsulated by the NPs, are important parameters for NP production. Drug loading obtained by coaxial turbulent jet mixer was higher than that reported for conventional bulk methods in literature,[7,32] notwithstanding that NPs synthesized by coaxial turbulent jet mixer are much smaller compared to conventional bulk methods. Drug loading and encapsulation efficiency obtained by coaxial turbulent jet mixer were comparable with those in NPs prepared by microfluidic hydrodynamic flow focusing (Figure 3b).[22] Also, encapsulation efficiency of insulin in PLGA−PEG NPs was lower compared to that of docetaxel, because insulin is charged and more hydrophilic than docetaxel (Figure 3b,d).

The coaxial turbulent jet mixer was also used for encapsulation of fluorescent dye molecules in lipid

TABLE 1. Total Flow Rate and Production Rate of PLGA−PEG NPs in a Coaxial Turbulent Jet Mixer at Different *Re*[a]

Reynolds number	1542	2570	3598
total flow rate	206.25 mL/min	343.75 mL/min	481.25 mL/min
production rate (10 mg/mL)	0.1875 g/min	0.3125 g/min	0.4375 g/min
production rate (50 mg/mL)	0.9375 g/min	1.5625 g/min	2.1875 g/min

[a] Here, the volumetric flow rate ratio of inner flow to outer flow was fixed at 0.1.

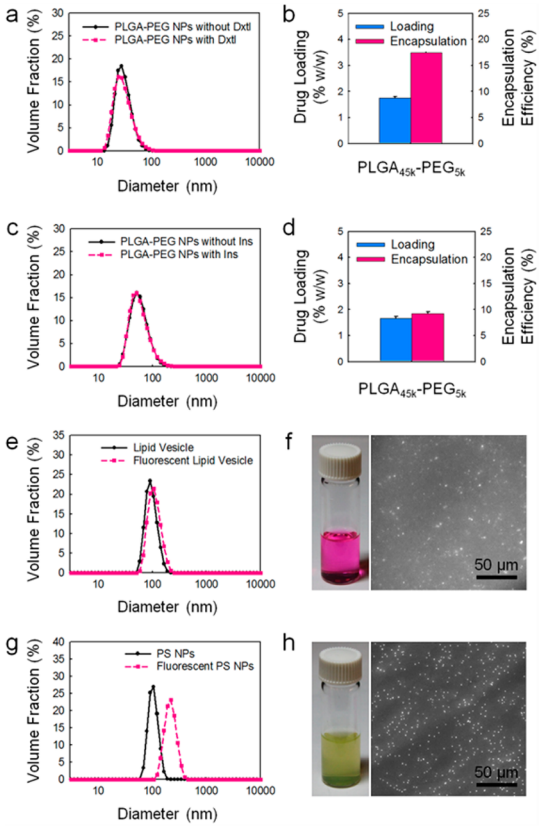

Figure 3. Encapsulation of drugs and fluorescent molecules in NPs prepared using the coaxial turbulent jet mixer. (a) Size distribution and (b) drug loading and encapsulation efficiency of $PLGA_{45k}$-PEG_{5k} NPs with docetaxel as a model therapeutic agent. (c) Size distribution and (d) drug loading and encapsulation efficiency of $PLGA_{45k}$-PEG_{5k} NPs with insulin as a model therapeutic agent. (e) Size distribution of lipid vesicles without and with $DiIC_{18}$ dye. (f) Photograph and fluorescence microscope image of lipid vesicles with $DiIC_{18}$ dye. (g) Size distribution of polystyrene NPs without and with perylene dye. (h) Photograph and fluorescence microscope image of polystyrene NPs with perylene dye. Error bars denote ± s.d.

vesicles and polystyrene NPs as model imaging agents (Figure 3e–h). When lipid vesicles were loaded with fluorescent dye molecules ($DiIC_{18}$), the average size of NPs increased slightly (Figure 3e) because $DiIC_{18}$ dye is a membrane intercalating dye.[15] On the other hand, the average size of polystyrene NPs increased significantly with encapsulation of fluorescent dye molecules (perylene) (Figure 3g), presumably because the hydrophobicity of perylene affects the NP assembly. Encapsulation of these fluorescent dye molecules was confirmed visually and by fluorescence microscopy (Figure 3f,h).

***In Vitro* Gene Knockdown by siRNA/PEI Polyplex NPs.** The coaxial turbulent jet mixer can overcome the issues of batch-to-batch reproducibility that are often a considerable challenge for scale-up of NP synthesis from the laboratory to clinical and industrial production.[1,8,9] We illustrate this with the example of siRNA, which has emerged as one of the strongest candidates for RNA interference therapy.[33] However, use of siRNA as a practical therapeutic agent is challenging due to its susceptibility to degradation by nucleases present in the body fluids, its relatively high molecular weight, and its anionic charge that limits cellular uptake and transport to the cytosol.[34] These challenges can be overcome by employing delivery systems or carriers. One of the promising approaches is by condensing the siRNA into a compact size by using counterion polyelectrolyte (*e.g.*, PEI, chitosan, *etc.*) to protect the activity of siRNA, to screen the negative charge for enhancement of the cellular accumulation, and to ensure endosomal escape of the siRNA for effective RNA interference.[27,35,36]

Similar to other polyelectrolyte interactions, siRNA/polycation polyplex NP formulations prepared by bulk synthesis method have limited uniformity, batch-to-batch reproducibility, and scalability. In case of the conventional bulk synthesis method, scale-up for the synthesis of siRNA/polycation polyplex NPs is a conundrum because the physicochemical properties of NPs are significantly altered as the batch size is increased for scale-up, as illustrated by the observed differences in the size distributions of polyplex NPs prepared in different batch sizes using the conventional bulk synthesis method (Figure 4a). In contrast, the coaxial turbulent jet mixer can synthesize siRNA/PEI polyplex NPs in a continuous and high-throughput manner, resulting in smaller NPs with narrower size distributions compared to those prepared by bulk synthesis (Figure 4a). The properties of NPs synthesized using the coaxial turbulent jet mixer are independent of the batch size (*i.e.*, amount of NPs synthesized) because the conditions for NP formation are identical and independent of the batch size for all NPs produced.

The transfection ability and resulting gene knockdown of siRNA/PEI polyplex NPs (molar ratio 1:3) were studied *in vitro* by using dual-luciferase (firefly and renilla) expressing HeLa cell line. In case of siRNA/PEI polyplex NPs synthesized by coaxial turbulent jet mixer, the luciferase expression was reduced by 50 and 60% at effective siRNA concentrations of 20 and 50 μM, respectively (Figure 4b). In case of commercially available transfection agent Lipofectamine 2000, however, the luciferase expression was reduced by only 5% at a siRNA concentration of 20 μM, but was brought down by 60% at siRNA concentration of 50 μM (Figure 4b). This result illustrates the utility of the coaxial turbulent jet mixer to ensure batch-to-batch reproducibility of siRNA/PEI polyplex NPs while maintaining the effectiveness for gene knockdown.

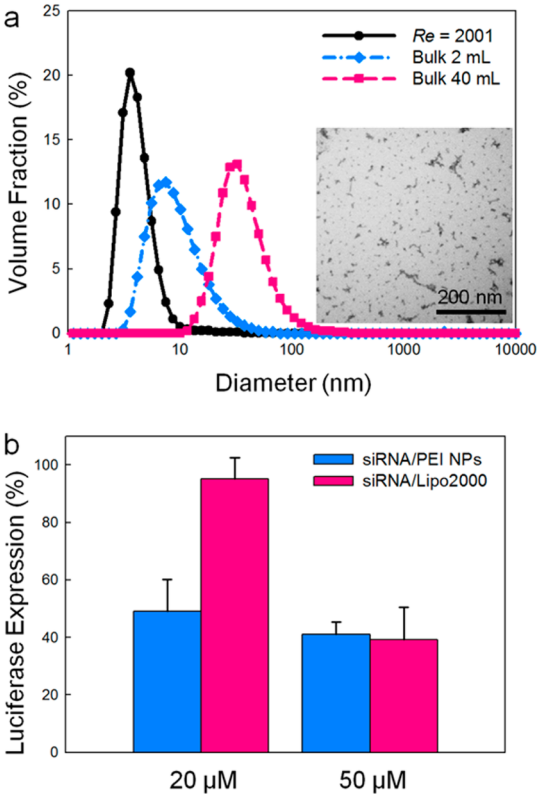

Figure 4. Reproducible preparation and effectiveness of siRNA/PEI polyplex NPs using the coaxial turbulent jet mixer. (a) Size distribution of siRNA/PEI polyplex NPs prepared by coaxial turbulent jet mixer, compared to bulk synthesis with different batch sizes (2 and 40 mL) that show variability in NP size. Inset shows the TEM image of siRNA/PEI polyplex NPs prepared by coaxial turbulent jet mixer. (b) Luciferase expression (%) in HeLa cells expressing both firefly and renilla luciferase, treated with NPs carrying GL3 siRNA, at various effective siRNA concentrations (*i.e.*, 20 and 50 μM) relative to scrambled siRNA, used as control. All results correspond to 2 days post-transfection, and are compared to commercially available transfection reagent Lipofectamine 2000. Cells treated with free siRNA had 100% luciferase expression. Error bars denote $\pm$ s.d.

DISCUSSION

The application of NPs synthesized by microfluidic platforms to large-animal *in vivo* and clinical studies has been challenging due to the intrinsic problem of low production rates.[1,2] A few millifluidic mixers have

been developed to overcome this drawback; however, they are not widely adopted in biomedical laboratories because fabrication of the millifluidic systems requires specialized micromachining.[14,24,25]

We developed a simple and versatile coaxial turbulent jet mixer for synthesis of various types of NPs. The coaxial turbulent jet mixer can be prepared within 30 min without any specialized equipment, microfabrication facilities, or specialized skills. In addition, the coaxial turbulent jet mixer can be made from standard fittings and materials that exhibit good solvent resistance. The fluid flow and mixing process does not require very precise alignment of the inner and outer tubes. To ensure that the inner tube is coaxially aligned with the outer tube (typically within 0.5 mm of the axis of the outer tube) we used metal syringe needle as the inner tube and fixed the outer flexible tubing on a rigid plate. The flow behavior in the coaxial turbulent jet mixer was captured as images and videos by systematically changing *R* and *Re* and summarized as phase diagram (Figure 1c). If there are significant differences in relative densities and viscosities of the inner and outer fluid, the inner stream can touch the inner wall of outer tube in the laminar flow regime. In the vortex and turbulence regime and turbulent jet regime, on the other hand, this effect is negligible because of fast lateral flow velocity of fluids. Since the coaxial turbulent jet mixer was operated in the turbulent jet regime for NP synthesis, the effect of small differences in relative densities and viscosities on NP synthesis is negligible. By flowing NP precursor and nonsolvent through inner and outer tubes, respectively, we can fix the ratio of NP precursor and nonsolvent, which is one of the important parameters that determines the NP size distribution. As proof of concept, we demonstrated the synthesis of PLGA–PEG NPs, lipid vesicles, iron oxide NPs, polystyrene NPs, and siRNA/PEI polyplex NPs, which are the major types of NPs widely used in biomedical applications. In addition, we demonstrated single-step encapsulation of various functional agents including anticancer drug, insulin, fluorescent dyes, and siRNA. The synthesized NPs could be easily recovered and separated by using ultrafiltration or freeze-dry method. We expect that this mixer design can be used to synthesize other types of NPs and microparticles.

The coaxial turbulent jet mixer can resolve the production rate issue without compromising on the controllability and reproducibility offered by microfluidic platforms. NP precursors are introduced through inner stream that is surrounded by the outer stream, mitigating direct precipitation on the surfaces. Moreover, since the high flow speed of the fluid washes away all precipitates toward collection bath, there is no buildup of precipitate onto the channel wall even after operation for a long time (Supporting Information Figure S4). The coaxial turbulent jet mixer could achieve a production rate up to 2.19 g/min, which is equivalent to 3.15 kg/d and 1.15 ton/yr. Considering that the production rates typically required for drug delivery applications in clinical studies and industrial-scale production of NPs are on the order of 0.1 and 1 kg/d, respectively, it is noteworthy that a single coaxial turbulent jet mixer can meet both requirements. In addition, controlled and rapid mixing in the coaxial turbulent jet mixer leads to more homogeneous and smaller NPs compared to those synthesized by conventional bulk synthesis methods. Since smaller NPs can penetrate more deeply into solid tumors,[37,38] the coaxial turbulent jet mixer has the potential to synthesize NPs with better drug delivery performance compared to conventional bulk methods. As a proof of concept, siRNA/PEI polyplex NPs were formulated using the coaxial mixer device, which could knock down the target gene more effectively as compared to a commercially available transfection agent at lower siRNA dose (Figure 4b). The coaxial turbulent jet mixer also allows for reproducible synthesis of NPs from quantities suitable for *in vitro* assays (requiring only a few seconds for synthesis) all the way up to industrial-scale production. One can also envision directly jetting the inner fluid into a stirred beaker for rapid mixing to provide better control over conventional nanoprecipitation in bulk, although the nanoprecipitation conditions will vary as the composition of the solution in the beaker changes with time. The ability to synthesize NPs at quantities over the entire range from initial benchtop screening all the way to manufacture obviates many of the issues regarding reoptimization of NP synthesis processes to account for changes in NP properties that usually occur with scale-up.

CONCLUSION

We reported a simple and versatile coaxial turbulent jet mixer that can synthesize various types of NPs with high production rates up to 3.15 kg/d. The coaxial turbulent jet mixer could be fabricated within 30 min without requiring specialized equipment, microfabrication facilities, or specialized skills, making it easily accessible to nanomedicine researchers. We characterized the fluidic behavior of this device to identify the turbulent jet regime where effective mixing is obtained, which occurs at Reynolds numbers above 500 and flow velocity ratios greater than 1. We further established the versatility of this platform by reproducibly synthesizing PLGA–PEG NPs, lipid vesicles, iron oxide NPs, polystyrene NPs, and siRNA/PEI polyplex NPs. We also encapsulated different functional agents including anticancer drug, insulin, fluorescent dyes, and siRNA. As a proof of concept, we performed *in vitro* gene knockdown study using siRNA/PEI polyplex NPs rapidly synthesized by the coaxial turbulent jet mixer, which are not easily synthesized in a reproducible manner by conventional methods. In summary, the coaxial turbulent jet mixer can be used as a versatile

platform for reproducible and controlled synthesis of NPs with high throughput suitable for large animal *in vivo* studies, clinical trials, and industrial-scale production. This technology has the potential to expedite the development and translation of new nanomedicines to the clinic for diagnostic and therapeutic applications, and to also impact bulk synthesis of NPs for a variety of other nonmedical applications.

METHODS

Fabrication of Coaxial Turbulent Jet Mixer. Tee union tube fittings made of clear polycarbonate (McMaster-Carr) or PTFE (Plasmatech Co.) were used for fabrication. A hole was drilled using a 0.025 in. diameter drill bit (#72, Drill bit city) and a 23 G blunt needle (337 μm I.D. and 641.4 μm O.D., Strategic applications Inc.) was inserted through the drilled hole and fixed by optical adhesive (NOA81, Norland products) and cured under UV light. Silastic tubing (VWR scientific products) or PTFE tubing (Plasmatech Co.) with inner diameters D = 3.175 mm were connected to the tee union tube fitting using a connector and adaptor (IDEX Health & Science).

Characterization of Mixing in the Coaxial Turbulent Jet Mixer. The device made from clear polycarbonate and transparent silastic tubes was used for the imaging and characterization of flow behavior in the coaxial turbulent jet mixer, since PTFE tee union and Teflon tubes are not transparent (Figure 1a,b). The flow rates were controlled by syringe pumps (Harvard Apparatus). Mixing of the inner and outer streams was visualized using phenolphthalein (Sigma-Aldrich). Because phenolphthalein is insoluble in water, 0.1 N sodium hydroxide (Sigma-Aldrich) in water−ethanol mixture (1:2 in volume ratio) with 1% w/v phenolphthalein was used as the pink colored basic inner solution. The composition of outer solution was 0.1 N hydrogen chloride (Sigma-Aldrich) in water−ethanol mixture (1:2 in volume ratio). To match the densities of inner fluid and outer fluid, same composition of water−ethanol mixture was used to prepare basic inner solution and acidic outer solution. As a result, the vertical buoyancy-driven drift of the inner fluid stream was negligible (Figure 1b). To estimate the *Re*, kinematic viscosity (ν) of water−ethanol mixture was calculated by using the previously reported values of dynamic viscosity (μ) and density (ρ) in water−ethanol mixtures.[39] Enhanced aluminum-coated right-angle prism mirror (Edmund optics, Inc.) was placed adjacent to the coaxial turbulent jet mixer to capture top and side views simultaneously, while the images and videos were taken from above the coaxial turbulent jet mixer. The flow in the coaxial turbulent jet mixer was captured as images and videos by systematically varying *R* and *Re*. *L* was determined by analyzing images in ImageJ, defined as the length at which the gray value of the green channel split from the image was 90% of the intensity difference between the completely mixed flow far downstream along the centerline and the tip of the inner syringe needle (Supporting Information Figure S1). In cases where the flow was still unmixed at the edge of right angle prism mirror (*i.e.*, in 75 mm), *L* was not estimated.

Preparation of PLGA−PEG NPs. $PLGA_{45k}$-PEG_{5k} and $PLGA_{95k}$-PEG_{5k} (Boehringer Ingelheim GmbH) was dissolved in acetonitrile (ACN, Sigma-Aldrich) at concentrations of 10 or 50 mg/mL. For the drug loading test, docetaxel (LC laboratories) and human recombinant insulin (Sigma-Aldrich) were used as model therapeutic agents. The PLGA−PEG precursor in ACN and deionized water were used as inner and outer stream, respectively. To make insulin loaded PLGA−PEG NPs, dimethyl sulfoxide (DMSO, Sigma-Aldrich) was used as organic solvent, because insulin is not soluble in ACN. During the NP synthesis, the flow rates were controlled by syringe pumps (Harvard Apparatus). To estimate the *Re*, ν of water−ACN mixture and water−DMSO mixture were calculated by using the previously reported values of μ and ρ in water−ACN mixtures and water−DMSO mixtures, respectively.[40,41] The output stream from the coaxial turbulent jet mixer was collected in a beaker. The resulting NP suspension was purified by ultrafiltration using Amicon Ultracel 100 K membrane filters. In case of bulk synthesis, 100 μL of polymeric precursor solution was mixed dropwise with 1 mL of water for about 2 h under magnetic stirring.

Preparation of Lipid Vesicles. Dimyristoylphosphatidylcholine (DMPC, Avanti Polar Lipids, Inc.), cholesterol (Avanti Polar Lipids, Inc.), and dihexadecyl phosphate (DCP, Sigma-Aldrich) were dissolved in a molar ratio of 5:4:1 in chloroform (Sigma-Aldrich). The chloroform was removed by evaporation under a stream of nitrogen gas at 30 °C. The glass vial with a dry lipid blend was stored in a desiccator for 24 h to remove residual chloroform. The lipid blend was dissolved in isopropyl alcohol (IPA) at concentration of 5 mM. To make fluorescent lipid vesicles, 1 wt % of 1,1′-dioctadecyl-3,3,3′,3′-tetramethylindocarbocyanine perchlorate (DiIC18, Sigma-Aldrich) with respect to the total weight of the lipid blend was added to the lipid blend in the IPA solution. The lipid blend in IPA solution and phosphate buffered saline (PBS) were used as inner and outer streams, respectively. To estimate the *Re*, ν of water−IPA mixture was calculated by using the previously reported values of μ and ρ in water−IPA mixtures.[42] In case of bulk synthesis, 100 μL of lipid blend in IPA solution was mixed dropwise with 1 mL of PBS for about 2 h under magnetic stirring.

Preparation of Iron Oxide NPs. Iron(II) chloride tetrahydrate and iron(III) chloride (Sigma-Aldrich) was dissolved in 1 N hydrochloric acid (Sigma-Aldrich) at concentration of 10 mM in a molar ratio Fe (II)/Fe (III) of 1:1. The iron oxide precursor in hydrochloric acid and alkaline solution of tetramethylammonium hydroxide (TMAOH, Sigma-Aldrich) at concentration of 172 mM were used as inner and outer streams, respectively. In case of bulk synthesis, 100 μL of iron oxide precursor in hydrochloric acid solution were mixed dropwise with 1 mL of TMAOH for about 2 h under magnetic stirring.

Preparation of Polystyrene NPs. Polystyrene (MW 35000, Sigma-Aldrich) was dissolved in tetrahydrofuran (THF, Sigma-Aldrich) at a concentration of 1 mg/mL. To make fluorescent polystyrene NPs, 10 wt % of perylene (Sigma-Aldrich) to the total weight of polystyrene was added to the polystyrene in THF solution. The polystyrene precursor in THF and deionized water were used as inner and outer streams, respectively. To estimate the *Re*, ν of water−THF mixture was calculated by using the previously reported values of μ and ρ in water−THF mixtures.[43] In case of bulk synthesis, 100 μL of polystyrene precursor solution was mixed dropwise with 1 mL of water for about 2 h under magnetic stirring.

Preparation of siRNA/PEI Polyplex NPs. The siRNA/PEI polyplex NPs were prepared by mixing aqueous solution of siRNA (Luciferase (GL3): sequence 5′-CUU ACG CUG AGU ACU UCG AdTdT-3′ (sense) and 5′-UCG AAG UAC UCA GCG UAA GdTdT-3′ (antisense)) and polyethylenimine ($PEI_{25k,Branched}$) at varying molar ratios (siRNA:PEI = 1:1 to 1:4). The aqueous siRNA solution and aqueous PEI solution were used as inner and outer streams, respectively. In case of bulk synthesis, 4 mL of aqueous siRNA solution and 40 mL of aqueous PEI solution was mixed by vortexing at 1500 rpm, at different concentrations so as to keep the desired molar ratios of siRNA and PEI as described above. The synthesized siRNA/PEI polyplex NPs were lyophilized and stored at −20 °C until use.

Characterization of NPs. The size distributions by volume fraction of the synthesized NPs and polystyrene microspheres (99 nm, Bangs laboratories, Inc.) were measured using dynamic light scattering with Zetasizer Nano ZS (Malvern Instruments, Ltd.). The synthesized NPs were imaged by TEM (JEOL 200CX). For TEM imaging, PLGA−PEG NPs and lipid vesicles were stained by uranyl acetate (Electron Microscopy Sciences). Docetaxel loading in the PLGA−PEG NPs were measured by HPLC (Agilent Technologies, 1100 Series) using established procedures.[32] Insulin loading in the PLGA−PEG NPs was measured by a protein bicinchoninic acid (BCA) assay (Lamda Biotech). Fluorescence images of lipid vesicles and polystyrene NPs were

acquired using an epi-fluorescence microscope (Eclipse TE 2000-U, Nikon). The typical sample volume for characterization was 15 and 1.1 mL for coaxial turbulent jet mixer and bulk synthesis method, respectively.

***In Vitro* Transfection.** All the *in vitro* transfection experiments were performed in quadruplicate. Dual-Luciferase (Luc) HeLa cells were grown and then seeded in 96-well plates at a density of 10000 cells/well 18 h before transfection. The cells were incubated for 24 h with various amounts of siRNA/PEI polyplex NPs in media without FBS. For all the NP treatments encapsulating GL3 siRNA, scrambled siRNA/PEI polyplex NP was used as negative control. Lipo2000/siRNA complex was formulated following the manufacturer's protocol (Invitrogen) and was used as a positive control for transfection. After the incubation period, the cells were washed with growth media and allowed to grow for a period of 24 h. The HeLa cells were then analyzed for expression of firefly and renilla luciferase signals by using the Dual-Glo Luciferase Assay System (Promega). The luminescence intensity was measured using a microplate reader (BioTek).

Conflict of Interest: The authors declare the following competing financial interest(s): In compliance with the Brigham and Women's Hospital and Harvard Medical School institutional guidelines, O.C.F. discloses his financial interest in BIND Therapeutics, Selecta Biosciences, and Blend Therapeutics, three biotechnology companies developing NP technologies for medical applications. BIND, Selecta, and Blend did not support the aforementioned research, and currently these companies have no rights to any technology or intellectual property developed as part of this research.

In compliance with MIT institutional guidelines, R.L. discloses his financial interest in BIND Therapeutics, Selecta Biosciences, Blend Therapeutics, and Kala, four biotechnology companies developing nanoparticle technologies for medical applications. BIND, Selecta, Blend, and Kala did not support the aforementioned research, and currently these companies have no rights to any technology or intellectual property developed as part of this research.

Acknowledgment. This research was supported by the Koch-Prostate Cancer Foundation Award in Nanotherapeutics (R.L. and O.C.F.), by the Concept Development Grant 5P50CA090381−09 from the Dana Farber Cancer Institute Prostate SPORE (O.C.F.), by NIH Grants EB015419 (O.C.F. and R.K.), CA119349 (R.L. and O.C.F.), and EB003647 (O.C.F.). We also thank Dr. N. Bertrand and Dr. I.-H. Lee for scientific discussions and insightful comments.

Supporting Information Available: Calculation of fluid velocities, method for determining the mixing time, size distribution comparison of iron oxide NPs and polystyrene NPs, effect of synthesis scale on size distribution of PLGA−PEG NPs, flow behavior in different flow regimes (video), and demonstration of NP production rate (video). This material is available free of charge *via* the Internet at http://pubs.acs.org.

REFERENCES AND NOTES

1. Valencia, P. M.; Farokhzad, O. C.; Karnik, R.; Langer, R. Microfluidic Technologies for Accelerating the Clinical Translation of Nanoparticles. *Nat. Nanotechnol.* **2012**, *7*, 623–629.
2. Kamaly, N.; Xiao, Z.; Valencia, P. M.; Radovic-Moreno, A. F.; Farokhzad, O. C. Targeted Polymeric Therapeutic Nanoparticles: Design, Development and Clinical Translation. *Chem. Soc. Rev.* **2012**, *41*, 2971–3010.
3. Rao, J.; Dragulescu-Andrasi, A.; Yao, H. Fluorescence Imaging *In Vivo*: Recent Advances. *Curr. Opin. Biotechnol.* **2007**, *18*, 17–25.
4. Santra, S.; Malhotra, A. Fluorescent Nanoparticle Probes for Imaging of Cancer. *Wiley Interdiscip. Rev.: Nanomed. Nanobiotechnol.* **2011**, *3*, 501–510.
5. Qiao, R.; Yang, C.; Gao, M. Superparamagnetic Iron Oxide Nanoparticles: from Preparations to *In Vivo* MRI Applications. *J. Mater. Chem.* **2009**, *19*, 6274–6293.
6. Shi, J.; Xiao, Z.; Kamaly, N.; Farokhzad, O. C. Self-Assembled Targeted Nanoparticles: Evolution of Technologies and Bench to Bedside Translation. *Acc. Chem. Res.* **2011**, *44*, 1123–1134.
7. Hrkach, J.; Von Hoff, D.; Ali, M. M.; Andrianova, E.; Auer, J.; Campbell, T.; De Witt, D.; Figa, M.; Figueiredo, M.; Horhota, A.; *et al.* Preclinical Development and Clinical Translation of a PSMA-Targeted Docetaxel Nanoparticle with a Differentiated Pharmacological Profile. *Sci. Transl. Med.* **2012**, *4*, 128ra139.
8. Murday, J. S.; Siegel, R. W.; Stein, J.; Wright, J. F. Translational Nanomedicine: Status Assessment and Opportunities. *Nanomedicine* **2009**, *5*, 251–273.
9. Marre, S.; Jensen, K. F. Synthesis of Micro and Nanostructures in Microfluidic Systems. *Chem. Soc. Rev.* **2010**, *39*, 1183–1202.
10. Wagner, J.; Köhler, J. M. Continuous Synthesis of Gold Nanoparticles in a Microreactor. *Nano Lett.* **2005**, *5*, 685–691.
11. Jahn, A.; Reiner, J. E.; Vreeland, W. N.; DeVoe, D. L.; Locascio, L. E.; Gaitan, M. Preparation of Nanoparticles by Continuous-Flow Microfluidics. *J. Nanopart. Res.* **2008**, *10*, 925–934.
12. Pan, J.; El-Ballouli, A. O.; Rollny, L.; Voznyy, O.; Burlakov, V. M.; Goriely, A.; Sargent, E. H.; Bakr, O. M. Automated Synthesis of Photovoltaic-Quality Colloidal Quantum Dots Using Separate Nucleation and Growth Stages. *ACS Nano* **2013**, *7*, 10158–10166.
13. Edel, J. B.; Fortt, R.; deMello, J. C.; deMello, A. J. Microfluidic Routes to the Controlled Production of Nanoparticles. *Chem. Commun.* **2002**, 1136–1137.
14. Johnson, B. K.; Prud'homme, R. K. Mechanism for Rapid Self-Assembly of Block Copolymer Nanoparticles. *Phys. Rev. Lett.* **2003**, *91*, 118302.
15. Jahn, A.; Vreeland, W. N.; Gaitan, M.; Locascio, L. E. Controlled Vesicle Self-Assembly in Microfluidic Channels with Hydrodynamic Focusing. *J. Am. Chem. Soc.* **2004**, *126*, 2674–2675.
16. Karnik, R.; Gu, F.; Basto, P.; Cannizzaro, C.; Dean, L.; Kyei-Manu, W.; Langer, R.; Farokhzad, O. C. Microfluidic Platform for Controlled Synthesis of Polymeric Nanoparticles. *Nano Lett.* **2008**, *8*, 2906–2912.
17. Jahn, A.; Stavis, S. M.; Hong, J. S.; Vreeland, W. N.; DeVoe, D. L.; Gaitan, M. Microfluidic Mixing and the Formation of Nanoscale Lipid Vesicles. *ACS Nano* **2010**, *4*, 2077–2087.
18. Valencia, P. M.; Basto, P. A.; Zhang, L. F.; Rhee, M.; Langer, R.; Farokhzad, O. C.; Karnik, R. Single-Step Assembly of Homogenous Lipid−Polymeric and Lipid−Quantum Dot Nanoparticles Enabled by Microfluidic Rapid Mixing. *ACS Nano* **2010**, *4*, 1671–1679.
19. Rhee, M.; Valencia, P. M.; Rodriguez, M. I.; Langer, R.; Farokhzad, O. C.; Karnik, R. Synthesis of Size-Tunable Polymeric Nanoparticles Enabled by 3D Hydrodynamic Flow Focusing in Single-Layer Microchannels. *Adv. Mater.* **2011**, *23*, H79–H83.
20. Kim, Y. T.; Chung, B. L.; Ma, M. M.; Muder, W. J. M.; Fayad, Z. A.; Farokhzad, O. C.; Langer, R. Mass Production and Size Control of Lipid-Polymer Hybrid Nanoparticles through Controlled Microvortices. *Nano Lett.* **2012**, *12*, 3587–3591.
21. Lim, J.-M.; Bertrand, N.; Valencia, P. M.; Rhee, M.; Langer, R.; Jon, S.; Farokhzad, O. C.; Karnik, R. Parallel Microfluidic Synthesis of Size-Tunable Polymeric Nanoparticles Using 3D Flow Focusing towards *In Vivo* Study. *Nanomedicine* **2014**, *10*, 401–409.
22. Valencia, P. M.; Pridgen, E. M.; Rhee, M.; Langer, R.; Farokhzad, O. C.; Karnik, R. Microfluidic Platform for Combinatorial Synthesis and Optimization of Targeted Nanoparticles for Cancer Therapy. *ACS Nano* **2013**, *7*, 10671–10680.
23. Lee, J. N.; Park, C.; Whitesides, G. M. Solvent Compatibility of Poly(dimethylsiloxane)-Based Microfluidic Devices. *Anal. Chem.* **2003**, *75*, 6544–6554.
24. Zhang, C.; Pansare, V. J.; Prud'homme, R. K.; Priestley, R. D. Flash Nanoprecipitation of Polystyrene Nanoparticles. *Soft Matter* **2012**, *8*, 86–93.

25. Shen, H.; Hong, S.; Prud'homme, R.; Liu, Y. Self-Assembling Process of Flash Nanoprecipitation in a Multi-Inlet Vortex Mixer to Produce Drug-Loaded Polymeric Nanoparticles. *J. Nanopart. Res.* **2011**, *13*, 4109–4120.
26. Abou Hassan, A.; Sandre, O.; Cabuil, V.; Tabeling, P. Synthesis of Iron Oxide Nanoparticles in a Microfluidic Device: Preliminary Results in a Coaxial Flow Millichannel. *Chem. Commun.* **2008**, 1783–1785.
27. Howard, K. A.; Kjems, J. Polycation-Based Nanoparticle Delivery for Improved RNA Interference Therapeutics. *Expert Opin. Biol. Ther.* **2007**, *7*, 1811–1822.
28. Bałdyga, J.; Bourne, J. R. *Turbulent Mixing and Chemical Reactions*; John Wiley & Sons: New York, 1999.
29. Lim, J.; Yeap, S.; Che, H.; Low, S. Characterization of Magnetic Nanoparticle by Dynamic Light Scattering. *Nanoscale Res. Lett.* **2013**, *8*, 381.
30. Farokhzad, O. C.; Jon, S.; Khademhosseini, A.; Tran, T.-N. T.; LaVan, D. A.; Langer, R. Nanoparticle-Aptamer Bioconjugates: a New Approach for Targeting Prostate Cancer Cells. *Cancer Res.* **2004**, *64*, 7668–7672.
31. Farokhzad, O. C.; Langer, R. Impact of Nanotechnology on Drug Delivery. *ACS Nano* **2009**, *3*, 16–20.
32. Cheng, J.; Teply, B. A.; Sherifi, I.; Sung, J.; Luther, G.; Gu, F. X.; Levy-Nissenbaum, E.; Radovic-Moreno, A. F.; Langer, R.; Farokhzad, O. C. Formulation of Functionalized PLGA-PEG Nanoparticles for *In Vivo* Targeted Drug Delivery. *Biomaterials* **2007**, *28*, 869–876.
33. de Fougerolles, A.; Vornlocher, H.-P.; Maraganore, J.; Lieberman, J. Interfering with Disease: A Progress Report on siRNA-Based Therapeutics. *Nat. Rev. Drug Discovery* **2007**, *6*, 443–453.
34. Whitehead, K. A.; Langer, R.; Anderson, D. G. Knocking down Barriers: Advances in siRNA Delivery. *Nat. Rev. Drug Discovery* **2009**, *8*, 129–138.
35. Swami, A.; Kurupati, R. K.; Pathak, A.; Singh, Y.; Kumar, P.; Gupta, K. C. A Unique and Highly Efficient Non-Viral DNA/siRNA Delivery System Based on PEI-Bisepoxide Nanoparticles. *Biochem. Biophys. Res. Commun.* **2007**, *362*, 835–841.
36. Malek, A.; Merkel, O.; Fink, L.; Czubayko, F.; Kissel, T.; Aigner, A. *In Vivo* Pharmacokinetics, Tissue Distribution and Underlying Mechanisms of Various PEI(−PEG)/siRNA Complexes. *Toxicol. Appl. Pharmacol.* **2009**, *236*, 97–108.
37. Cabral, H.; Matsumoto, Y.; Mizuno, K.; Chen, Q.; Murakami, M.; Kimura, M.; Terada, Y.; Kano, M. R.; Miyazono, K.; Uesaka, M.; *et al.* Accumulation of Sub-100 nm Polymeric Micelles in Poorly Permeable Tumours Depends on Size. *Nat. Nanotechnol.* **2011**, *6*, 815–823.
38. Chauhan, V. P.; Stylianopoulos, T.; Martin, J. D.; Popovic, Z.; Chen, O.; Kamoun, W. S.; Bawendi, M. G.; Fukumura, D.; Jain, R. K. Normalization of Tumour Blood Vessels Improves the Delivery of Nanomedicines in a Size-Dependent Manner. *Nat. Nanotechnol.* **2012**, *7*, 383–388.
39. Khattab, I.; Bandarkar, F.; Fakhree, M.; Jouyban, A. Density, Viscosity, and Surface Tension of Water+Ethanol Mixtures from 293 to 323K. *Korean J. Chem. Eng.* **2012**, *29*, 812–817.
40. Cunningham, G. P.; Vidulich, G. A.; Kay, R. L. Several Properties of Acetonitrile-Water, Acetonitrile-Methanol, and Ethylene Carbonate-Water Systems. *J. Chem. Eng. Data* **1967**, *12*, 336–337.
41. LeBel, R. G.; Goring, D. A. I. Density, Viscosity, Refractive Index, and Hygroscopicity of Mixtures of Water and Dimethyl Sulfoxide. *J. Chem. Eng. Data* **1962**, *7*, 100–101.
42. Lebo, R. B. Properties of Mixtures of Isopropyl Alcohol and Water. *J. Am. Chem. Soc.* **1921**, *43*, 1005–1011.
43. Pinder, K. L. Viscosity of the Tetrahydrofuran-Water System. *Can. J. Chem. Eng.* **1965**, *43*, 274–275.